

Flexible strain sensors based on epoxy/graphene composite film with long molecular weight curing agents

Qingshi Meng ¹, Yu Zhao,¹ Zhiwen Liu,¹ Sensen Han,¹ Shaowei Lu,¹ Tianqing Liu ^{1,2}

¹Faculty of Aerospace Engineering, Shenyang Aerospace University, Shenyang 110136, China

²QIMR Berghofer Medical Research Institute, Brisbane, Queensland 4006, Australia

Correspondence to: S. Lu (E-mail: lushaowei_2005@163.com) and T. Liu (E-mail: michelle.tianqing.liu@gmail.com)

ABSTRACT: Flexible strain sensors based on epoxy/graphene composite film with long molecular weight curing agents have critical roles in the development of advanced polymer composite films that combine mechanical robustness with functional properties such as electrical conductivity for many applications. In this experiment, flexible epoxy/GnP composite film is obtained by using flexible curing agent J2000. A percolation threshold of electrical conductivity was observed at merely 0.97 vol% GnPs, and the composite electrical conductivity increased to 10^{-6} S/cm at 5.0 vol %. The composite films were mechanically strong enough to be used as a flexible strain sensor. Our sensor can clearly detect the stretching of the forearm skin caused by a fist pulse and back of hand movement and achieve an enhancement of the resistance signal of up to 50%. When the GnPs content reaches 5%, Young's modulus and tensile strength increase to 21 MPa and 1.3 MPa, respectively. © 2019 Wiley Periodicals, Inc. *J. Appl. Polym. Sci.* **2019**, *136*, 47906.

KEYWORDS: epoxy; flexible sensor; graphene composite film

Received 16 December 2018; accepted 28 March 2019

DOI: 10.1002/app.47906

INTRODUCTION

Recently, high-performance multifunctional polymer composite films have attracted extensive attention in both academia and industry^{1–4} for potential applications in aerospace, automobile, construction, energy applications, and other emerging industries.^{5–9} Polymer composite films can be used to fabricate thin, lightweight, flexible, wearable sensors by combining matrix with functional materials.

As strain sensors can detect the mechanical deformations or structural changes, it is highly desirable to be used as a wearable device to record human physical motion for disease diagnosis, therapy, and health conditions monitoring.^{10,11} In most cases, strain sensors are based on piezo-resistance theory to translate mechanical deformations into resistance changes by strain gauge. Currently, rigid materials such as copper-nickel alloy and nichrome widely used as strain gauges of the sensors to achieve highly accuracy and large-scale industrial production.^{12,13} However, the main drawback of these sensors is the rigid feature of the materials, which limited their application to detect the deformation, damage, and structural changes of parts with large surface area or complex curve surface structure. Thus, there is a need to develop functional composite films that not only have good flexibility and mechanical properties but also have good conductivity and sensor properties.

Particles or materials with conductive and/or mechanical properties have been incorporated into the matrix to effectively improve

the properties of the matrix, such as mechanical, electrical, and sensing properties. Various conductive materials including metal nanostructures (gold nanoparticles, gold and silver nanowires) and carbon-based materials (graphene, carbon nanotubes [CNTs], and carbon black) have been extensively studied for fabrication of composite films. Nevertheless, metal-based sensors normally have poor stretch-ability and undesirable weight issues.⁸ Carbon-based materials, for example, graphene, fullerene (C60), CNTs, have good compatibility with polymers and thus are often used as fillers in composites. Nevertheless, carbon nanotubes are not yet used commercially for reinforcing or toughening polymers, because of expensive manufacturing costs (especially for single wall carbon nanotubes), high viscosity caused by the “bird’s nest” structure of the entangled tubes, and high anisotropic functionality.^{14,15} By comparison, graphene is an electrically and thermally conductive material with large specific surface area ($2630 \text{ m}^2 \text{ g}^{-1}$).¹⁶ It is stronger and stiffer than diamond and can elongate a quarter of its length. Its Young's modulus ($\sim 1 \text{ TPa}$), mechanical strength ($\sim 130 \text{ GPa}$) and electrical conductivity (up to 6000 S/cm) is as high as those of CNTs,^{17–19} whereas the manufacturing cost of graphene is expected to be much lower than those of CNT.

There are many polymer materials used as the matrix including polyurethanes,²⁰ poly(ethylene vinyl acetate)²¹ and epoxy resins.²² Epoxy resins are by far one of the most widely used polymer materials as structural adhesives, coating and molded materials,

and fabrication of functional composites.^{23–25} This is due to their excellent chemical resistance against severe corrosive conditions, high thermal and mechanical properties, excellent adhesion to a wide range of materials and ease of processing. Nevertheless, a major obstacle is that the addition of rigid particles promotes reduction of the epoxy ductility, making it more brittle.²⁶ The flexible curing agent J2000, a polyether amine with average molecular weight of 2000, can co-react in an epoxy system and solve this problem effectively. Their long molecular chains with primary amine groups can attach more functional particles to improve the uptake of functional particles. In addition, the cured composite has good flexibility and ductility. Several studies have reported that epoxy nanocomposites fabricated with J2000 and graphene-based particle materials can improve the thermal and electrical properties of epoxy resin.^{27,28}

This article presents a simple and facile approach to the fabrication of composite thin films that allows incorporating different graphene content into an epoxy matrix. These composite films not only have excellent mechanical and electrical properties but also have good flexibility. This makes them ideal for sensing body motion and monitoring such as pulse movement and muscle deformation.

EXPERIMENTAL SECTION

Materials

Acid-treated graphite, Asbury 1721, was kindly provided by Asbury Carbons (Asbury, NJ). Epoxy resin of commercial grade, diglycidyl ether of bisphenol A (DGEBA, Araldite-F) with epoxide equivalent weight 180–210 g per equiv., was purchased from Yanshan Co., Ltd. (China). Hardener Jeffamine D 2000 (denoted J2000, polypropylene oxide α,ω -diamine, Mw = 1968 g/mol) was purchased from Huntsman Advanced Materials (Singapore).

Graphene Platelets

Graphene platelets (GnPs) were fabricated according to a reported procedure.²⁹ In brief, 0.1 g graphite intercalation compound (GIC, Asbury 1721) was thermally shocked by transferring it into a preheated crucible at 700 °C in a furnace and incubated for 1 min. The expanded product was cooled and resuspended in acetone and then ultrasonicated for 2 h under 20 °C to promote the exfoliation of graphite.²⁹ GnPs were precipitated and collected for further usage.

Epoxy/GnP Composite Films

Four epoxy/GnP composite thin-films were prepared with various GnPs contents (1.25, 2.5, 3.75, and 5% GnPs). GnPs was dissolved in an epoxy acetone mixed solution with the weight ratio of 1:1. Hardener J2000 was added to the mixture at the ratio of 3:1 to epoxy, followed by stirring for 30 min, and sonicating for 1 h. After the acetone volatilized, the conductive mixtures were poured into a dumbbell shaped mold and then solidified in an oven at 120 °C for 12 h to produce solid epoxy/GnP composites. The processing of the composites is depicted schematically in Figure 1.

Morphology

Scanning electron microscope (SEM) was conducted using a SEM (JEOL JSM-7800F) with an accelerating voltage of 5 kV to examine the composite films' cross-section and surface. The thickness of the composite films was measured with a digital micrometer.

Mechanical Property

Tensile dumbbell samples were made using a silicone rubber mold. We prepared samples for mechanical testing according to the test standards of ASTM D 638-2003. Both sides of sample were polished by emery paper until all visible marks disappeared. Tensile testing was performed using an Instron 5567 tensile machine at 0.5 mm/min speed at room temperature. An Instron extensometer 2630-100 was used to collect accurate displacement

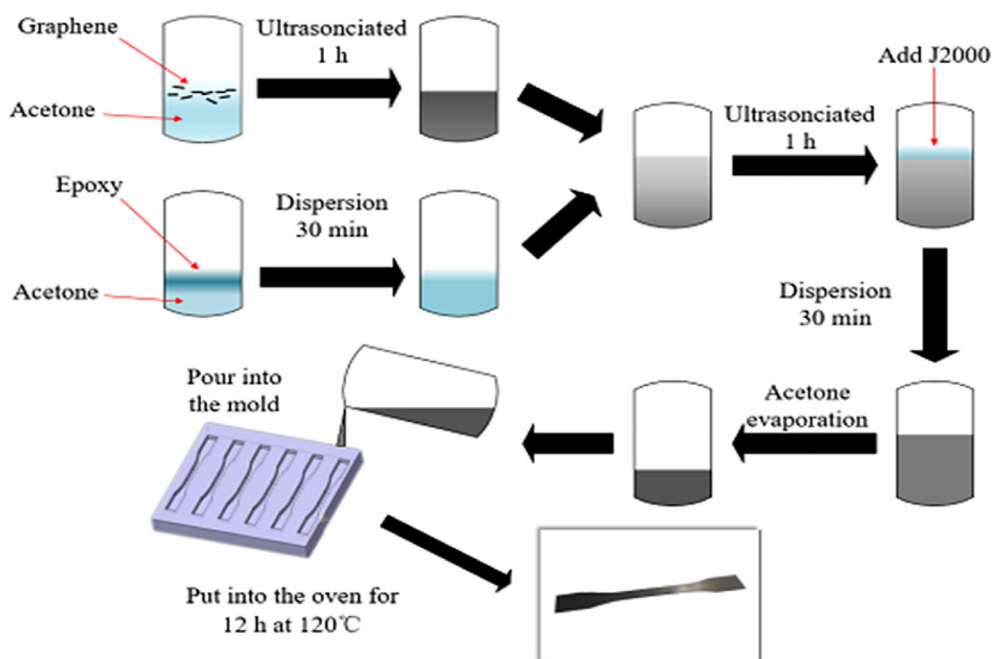


Figure 1. Schematic diagram of the fabrication of the epoxy/GnP composite film. [Color figure can be viewed at wileyonlinelibrary.com]

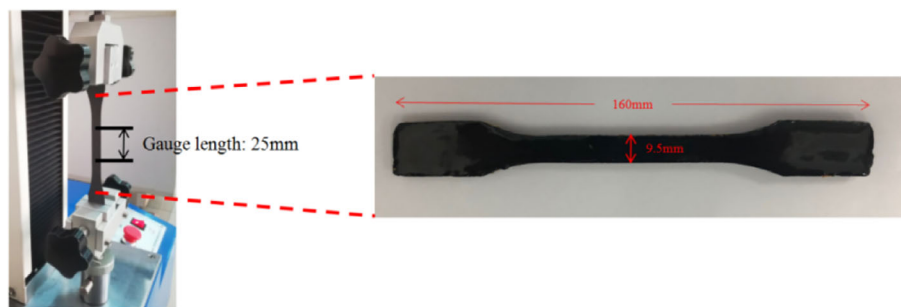


Figure 2. Mechanical testing and epoxy/GnP composite dumb-bell sample. [Color figure can be viewed at wileyonlinelibrary.com]

data for the modulus measurement which was calculated using 0.05–0.2% strain. The experimental setup for mechanical testing and the drum-bell composite is shown in Figure 2.

Electrical Properties

A square film (60 mm length of side, 0.5 mm thick) was placed between the electrodes of the resistor box. The upper electrode was adjusted to the correct position. After closing the resistance box cover, the load knob was adjusted to apply a pressure of about 10 kg onto the test sample. The electrical conductivity of the films was examined with a high resistance meter (Agilent 4339B) connected to a Keysight 16008B resistivity cell. Figure 3 is the setup of the conductivity testing. Figure 3(a) is high resistance meter and epoxy/GnP composite test sample, Figure 3(b) is the schematic diagram of conductivity testing.

Sensing Performance

Sensor property was evaluated based on piezo-resistance theory through the electrical resistance change from the conductive network within the sensor. The electrical resistance of sensor was monitored using a FLUKE 2638A HYDRA Series III Data Acquisition System (DAQ). Tensile testing was performed using an Instron 5567 tensile machine at 2 mm/min speed at room temperature.

The gauge factor (GF) was used to express the sensitivity of the strain sensor and is defined as the ratio of the rate of change of the relative resistance to the applied tensile strain. The normalized value of GF of the composite membrane can be determined by the eq. (1).

$$GF = \frac{\Delta R/R_0}{\Delta L/L_0} \quad (1)$$

where R_0 is the initial resistance of the sensor prior to straining, ΔR is the resistance change under the deformation, L_0 is the initial length of the sensor, and ΔL is the elongation of the axial specimen. The normalized resistance change $\Delta R/R_0$ is used to investigate the sensitivity of the epoxy/GnP flexible sensors.³⁰ The gauge factor was measured using an Instron Tensile Machine to provide the strain and the DAQ to monitor the changes of electrical resistance.

Motion and Bending Measurement

Motion and bending measurement response testing were performed and the DAQ was used to measure the electrical resistance changes of sensor under different movements and bending angles.

RESULTS AND DISCUSSION

Topographic Characterization of GnPs

The GnP morphology was observed by TEM [Figure 4(a)]. Large GnPs were observed to sit on a lacey-carbon film on a copper TEM grid, clearly illustrating the flake-like structure. There were some overlapped structures located at the right side of the image without lacey-carbon support. The most transparent and featureless region (red arrows in Figure 4(a)) likely possesses ultra-thin crystal structure, where we randomly selected a point (indicated by blue arrow) to examine the electron diffraction (ED) pattern (its ED pattern shows a typical six-fold symmetry expected for highly crystalline structure [Figure 4(b)]. In addition, its diffraction illustrates a stronger outer

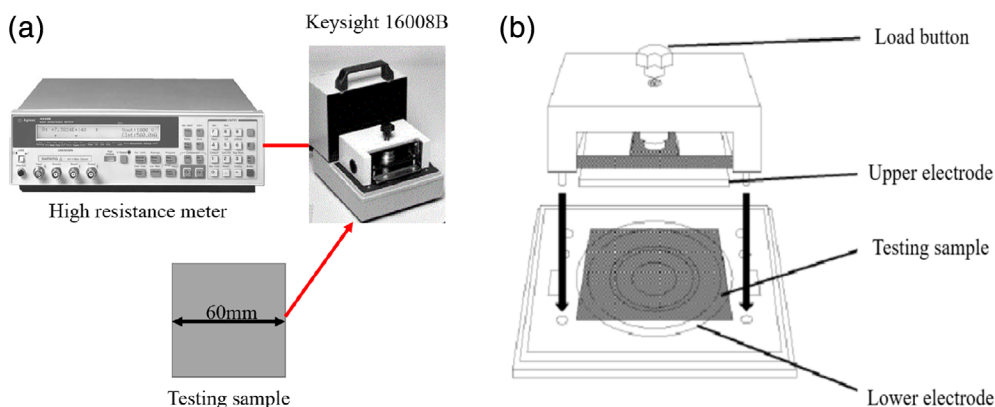


Figure 3. (a) High-resistance meter and epoxy/GnP composite test sample; (b) schematic diagram of conductivity testing. [Color figure can be viewed at wileyonlinelibrary.com]

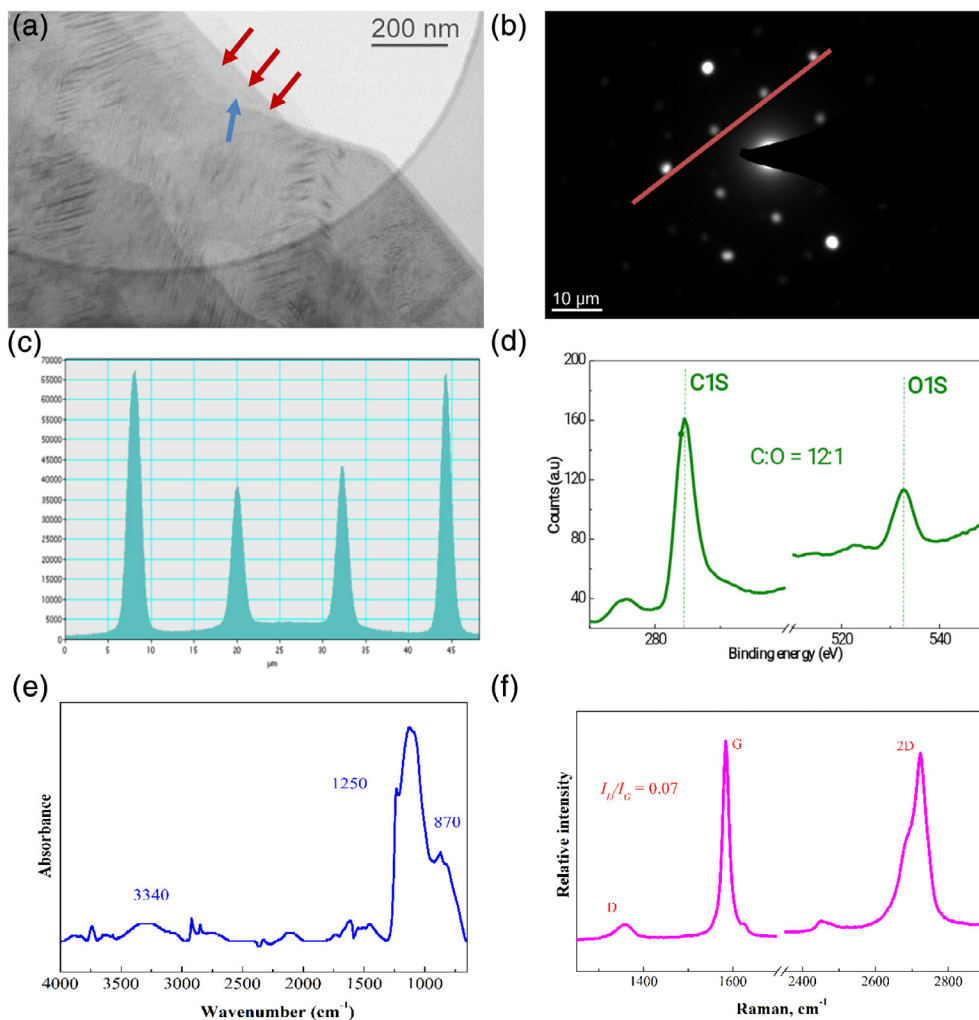


Figure 4. TEM images of GnPs fabricated by thermo-sonication method: (a) an overview of GnP structure; (b) electron diffraction pattern taken from with the peaks labeled by Miller-Bravais indices, and (c) diffraction intensity of double or triple layer graphene taken along the 1–210 to 0–110 axis; (d) XPS analysis; (e) FTIR spectra of GnPs; and (f) Raman spectra of GnPs. [Color figure can be viewed at wileyonlinelibrary.com]

intensity than inner [Figure 4(c)], confirming that the region contains few layers of graphene sheets.^{31,32} The high crystalline structure of GnPs is in agreement with the XPS analysis [Figure 4(d)], which shows a C/O ratio of 12:1. FT-IR spectra of GnPs showed that GnPs have absorptions at 3340, 1250, and 870 cm^{-1} , corresponding to —OH, —COOH, and epoxide groups, respectively [Figure 4(e)]. Raman spectra of GnPs demonstrated that GnPs have obvious absorptions at 1340, 1585, and 2690 cm^{-1} which correspond to D, G, and 2D bands, respectively [Figure 4(f)]. G band refers to sp^2 resonance on an ordered graphitic lattice, whereas D band is activated from the first-order scattering process of sp^2 carbons by the presence of in-plane substitutional hetero-atoms, vacancies, grain boundaries, or other defects, which might be sp^3 hybridized carbon structure associating with the quantity of impurity or oxidation degree. Because all samples were tested in the form of powder, there is no point to discuss 2D band.

Topographic Characterization of Epoxy/GnP Composite Films

We firstly synthesized GnPs using the previously mentioned method. The epoxy/graphene composite thin-films were fabricated

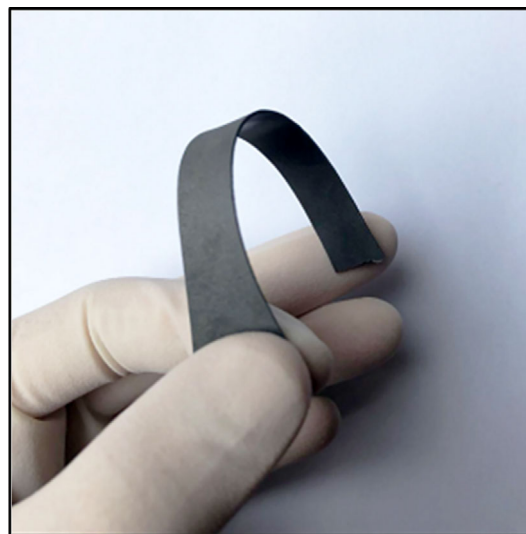


Figure 5. Bending the epoxy/GnP composite film. [Color figure can be viewed at wileyonlinelibrary.com]

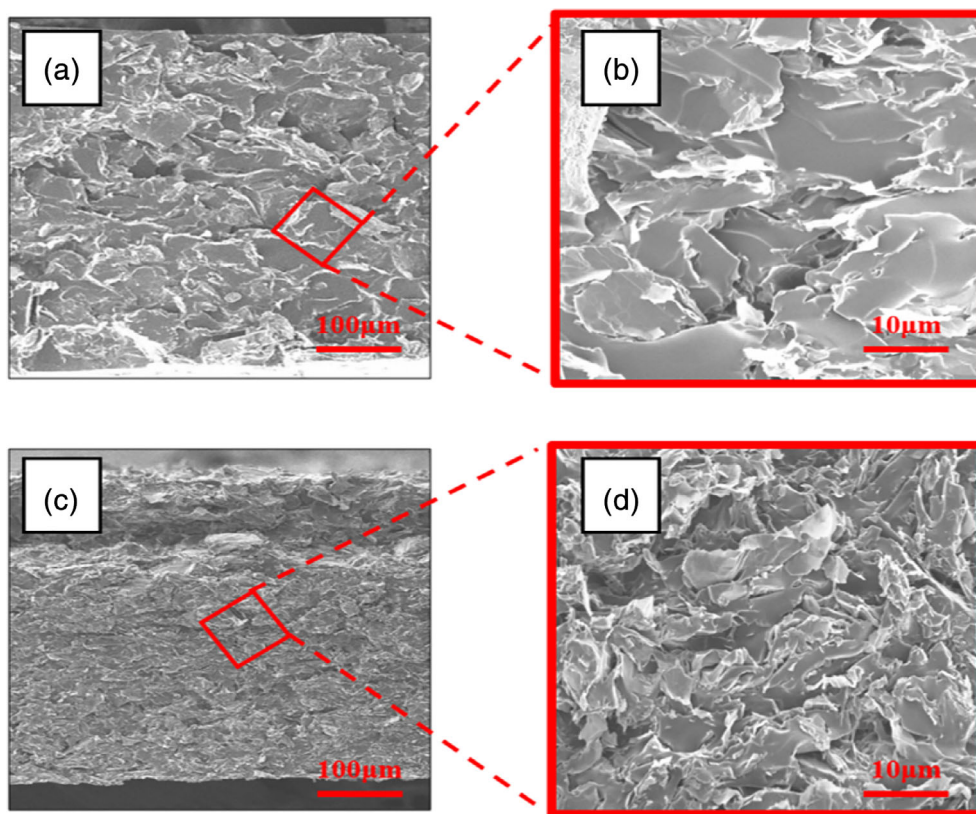


Figure 6. SEM images of epoxy/GnP nanocomposite film with 1.25% (a, b) and 5 vol % (c, d): (a) cross-sectional morphology of the epoxy/GnP composite film; (b) structure of GnPs; (c) cross-sectional morphology of the composite film; and (d) structure of GnPs. [Color figure can be viewed at wileyonlinelibrary.com]

with different concentrations of GnPs and solidified to be dumbbell shape using J2000 epoxy as a curing agent. The composite films' thickness is 0.5 mm. J2000 can be used in preparation of epoxy/graphene composites taking advantages of its high reactivity with graphene due to the two-terminal amine groups.²⁷ In the film, GnPs are dispersed evenly in the epoxy resin, and the film is solidified due to the effect of curing agent. The composite films we manufactured are flexible to bend due to the addition of a flexible curing agent J2000, as shown in the Figure 5.

To understand fracture mechanisms of the epoxy/GnP, the SEM micrographs were taken for epoxy/GnP composite films with different GnPs content. The lowest (1.25%) and highest (5%) GnPs contents were compared to show the differences in their structural changes (Figure 6). Layer breakage and cracks were observed in both composite films. The GnPs disperses in the thin film and connect tightly with each other, leading to enhanced electrical conductivity and mechanical properties. In comparison with Figure 5(b) and (d), it indicates that higher GnPs content in the composite films can increase fracture roughness of the materials, therefore leading to increased total contact surface area of the composites. Based on the data, the toughening mechanisms of those composites are described in details. When a tensile force was applied to the specimen, a high level of stress accumulated at the sharp crack tip, leading to increased local tension. Because J2000-cured epoxy is relatively ductile, stress mainly accumulates around the GnPs due to the difference in modulus and Poisson ratio between epoxy and GnPs. With continued

tensile loading of the specimen, fracture can initiate either at the interface between GnPs and matrix (data not shown) or on the surface of GnPs where voids, layer breakage, and micro-cracks are formed [Figure 6(b) and (d)]. In summary, because high content GnPs produced a rougher surface and stronger binding with the matrix compared with low content GnPs, high-content GnPs were able to carry more loading upon fracture.

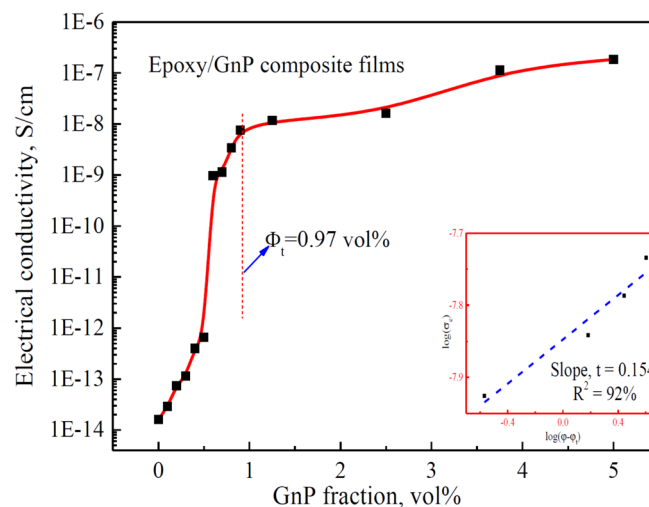


Figure 7. Through-plane electrical conductivity of epoxy/GnPs nanocomposite films. [Color figure can be viewed at wileyonlinelibrary.com]

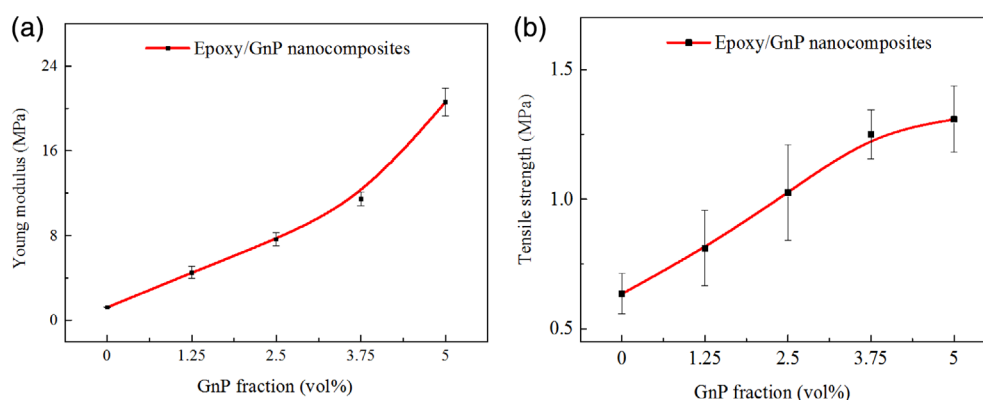


Figure 8. Young's modulus and tensile strength of epoxy/GnP nanocomposites with different GnPs content: (a) Young's moduli and (b) tensile strength. [Color figure can be viewed at wileyonlinelibrary.com]

Electrical Properties

Polymeric materials having electrical conductivity over 10^{-9} S/cm are recognized as a semi-conductive in engineering applications.³³ Because epoxy resins are extensively used in aerospace and electronics industries, it is of significance to improve their electrical resistance/conductivity by integrating them with conductive nanomaterials.^{34–37} The electrical properties of polymer composites mainly depend on the filler conductivity, geometry, fraction, dispersion, and interaction with matrices. The high-electrical conductive GnPs adopted in this study have a number of surface functional groups such as epoxide groups, which make it easier to be suspended in solvent. No further modification was made to minimize surface defects. Hence, the dispersion and fraction of GnPs in the composites are crucial to determine the final electrical properties of epoxy/GnP composites.

We have produced 14 sets of GnPs conductive films with GnPs content ranging from 0 to 5 vol % GnPs. The logarithm electrical conductivity change of different volume fraction of GnPs is shown in Figure 7. When 5 vol % of GnPs is added, the conductivity improved from 10^{-14} to 10^{-6} S/cm. At low volume fraction

(<0.7 vol %), the logarithm electrical conductivity amplitude exhibited negligible changes, whereas for 0.97 vol %, the logarithm electrical conductivity increased drastically. According to the classical percolation theory, the conductivity of the composite increases with increasing conductive filler content. This phenomenon can be described by the scaling law in the form of $\sigma = \sigma^0(c - c^*)^t$, where c^* is expressed as the percolation threshold, and σ^0 and t as the fitting parameters. This model provides a simple method suitable for comparison of experimental data.^{36,38,39} Electrical conductivity increased when mass fraction increased until the percolation threshold exceeded. By plotting the experimental data as $\log \sigma \propto \log(c - c^*)$, a suitable fit to this law can be found by changing c^* incrementally until the best linear fit to the equation is found.⁴⁰ The inset of Figure 7 shows the log–log plot of the equation, by fitting experimental data into the power law equation, we obtained a percolation threshold (the formation of pathways for electron transfer) of 0.97 vol % GnPs and an R^2 value of 92%.

Mechanical Properties

Young's modulus and tensile strength are measured to define the mechanical properties of the epoxy/GnP composites. Figure 8(a) shows the Young's moduli of neat epoxy and its nanocomposites with GnPs concentrations from 1.25 to 5 vol %. Epoxy/GnP composites showed prominent increase in modulus with the increases in GnPs concentrations. It increased 1700% when using 5 vol % GnPs in the composites compared with the neat epoxy resin controls. This may be caused by nanosized GnPs providing more specific surface area and interfacial structure that can effectively prevent stress concentrations and facilitate stress transfer across the interface

Table I. Elongation Break of Epoxy/GnP Nanocomposites

GnP fraction (vol %)	Strain (%)
1.25	15.09 ± 5.18
2.5	12.36 ± 1.10
3.75	11.44 ± 0.55
5	6.81 ± 1.20

Table II. A Comparison of Mechanical and Functional Performance of Various Similar Composite Films

Materials	Filler type	Hardeners	Tensile strengths, MPa	Young's moduli, MPa	Ref.
Epoxy composites	GnPs (1.25 vol %)	J400	21	1100	Our research
	GnPs (1.25 vol %)	J230	57–60	3200–3500	27
Silicone rubber	GnPs (1.25 vol %)	/	6.5–8.5	1.7–2.3	43
Styrene butadiene rubber	GnP (1.25 vol %)	Compound curing chemicals	6.5–7.5	1.3–1.7	44
Epoxy composites	GnPs (1.25 vol %)	J2000	0.6–1	4.5	Our research

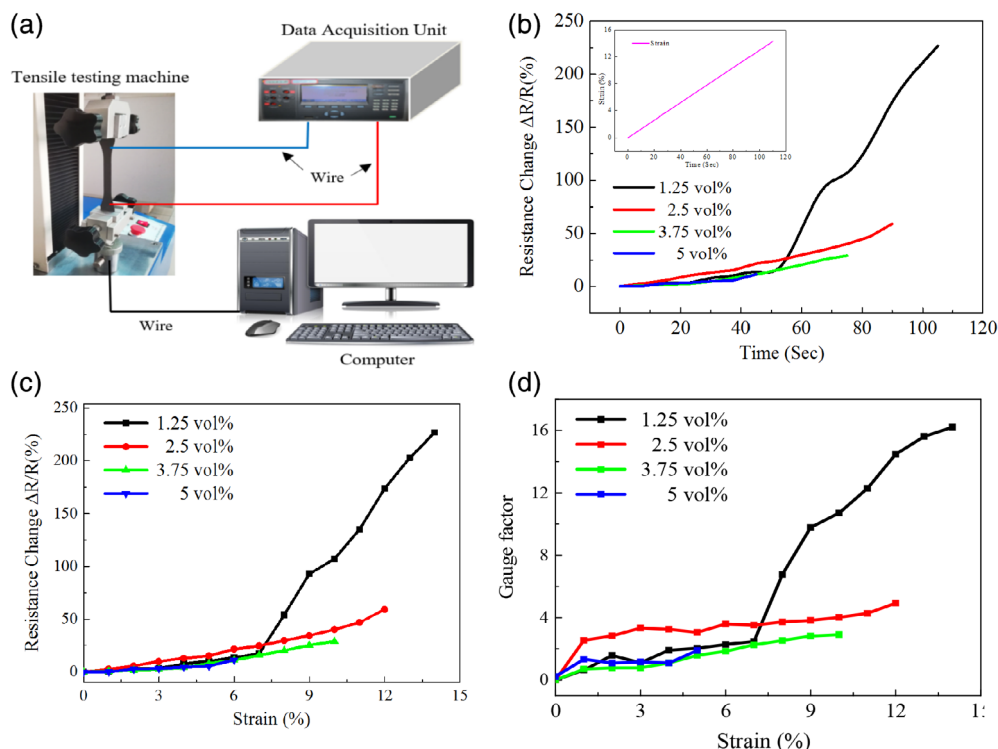


Figure 9. Gauge factor testing of strain sensor based on GnP composite films with different content: (a) the schematic of gauge factor testing; (b) the curves of resistance change versus time; (c) the curve of resistance changes and strain; and (d) the curves of gauge factor and strain. [Color figure can be viewed at wileyonlinelibrary.com]

under loading. Figure 8(b) demonstrated changes of the tensile strength of epoxy/GnP nanocomposites with the increase of GnPs concentration ranging from 1.25 to 5 vol%. An obvious increase in tensile strength was observed with the increase of GnPs in the epoxy/GnP composites, about 200% increase when using 5 vol % GnPs compared with the neat epoxy controls. Based on the previous research,^{38,41,42} the tensile strength is often reduced when a brittle matrix hardener is added. The opposite trend reported here is possibly because when adding GnPs into the resin matrix during the preparation of composite materials, GnPs achieved

good dispersion in the resin and better interaction with resin, resulting in dramatic sensitivity and improved mechanical properties.^{29,34} However, tensile strength slowly increased when the GnPs content is more than 3.75%. The possible reason is that part of GnPs aggregated at high concentration in the resin so that the GnPs and the resin matrix cannot be fully contacted and defects occur. Because of the difficulty in dispersing the graphene when its content is greater than 5 vol %, the experiment was conducted using GnPs up to 5 vol %. We have also summarized the elongation of the break in Table I and a comparison of the mechanical and functional performance of various similar composites in Table II.

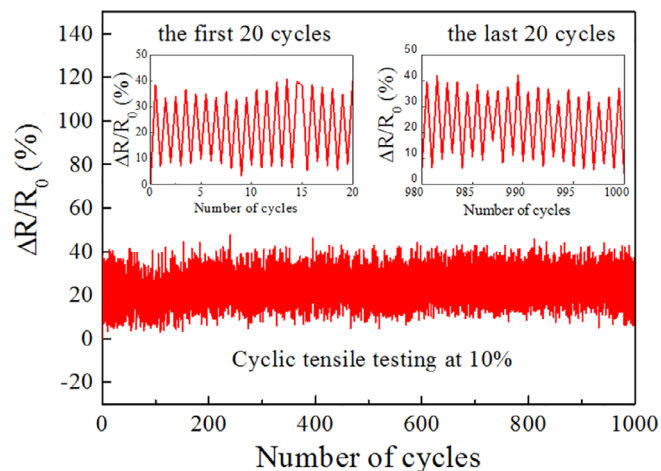


Figure 10. Cyclic tensile test of sensor at 10%. [Color figure can be viewed at wileyonlinelibrary.com]

As shown in Table II, we compared the mechanical properties of our epoxy/GnP composite film cured by J2000 with those of J230 and J400 cured composites. Our film shows relatively lower modulus and tensile strength than J230 and J400 cured epoxy/GnP composites, but it demonstrates better flexibility (Figure 5). Because our films are cured by the long chain molecular of J2000, promoting to creation of a ductile composite matrix. It is worth to compare our J2000 cured composite film with some GnP composites with ductile matrices such as rubbers (Table II).

Application of Strain Sensors

Strain sensors with high sensitivity can be used to measure electrical signal changes when small deformation occurs. This makes these sensors ideal monitoring human movement and other health-related parameters. The sensitivity is the key property for a strain sensor and affects the performance of strain sensor directly. Therefore, the gauge factor was used to investigate the sensitivity of strain

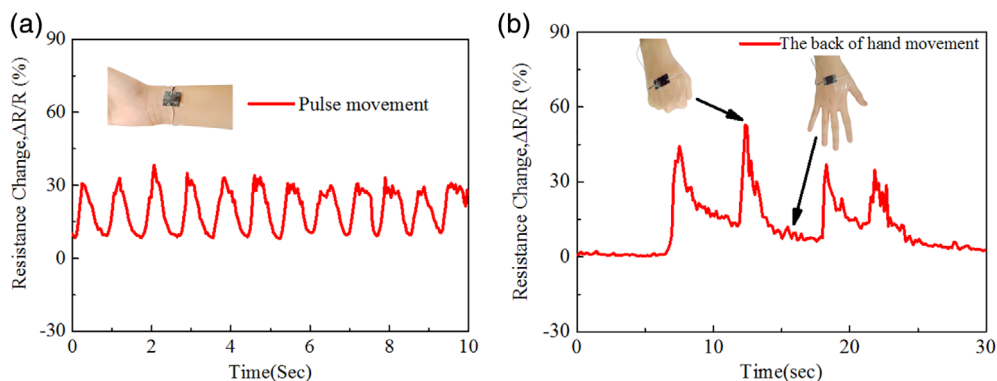


Figure 11. Strain sensor used to monitor (a) real-time pulse movement, and (b) back of hand movement. [Color figure can be viewed at wileyonlinelibrary.com]

sensor. Tensile tests of different GnPs content were performed to monitor induced electrical resistance changes to register the electrical response of the material under strain. Figure 9(a) is a schematic of the gauge factor test in which the conductive resistance was measured during the tensile test. To find the optimal sensitivity, a number of GnPs composite films with different GnPs content were examined to obtain their gauge factors. The resistance changes curves of flexible sensor at various ratios of GnPs and the strain versus time was measured by DAQ and Instron 5567 tensile machine, respectively [Figure 9(b)]. We then combined the strain and resistance change at same time to obtain Figure 9(c). Figure 9(c) shows the relationship between electrical resistance changes of GnPs composite films with different contents and tensile strain. The results show the electrical resistance increases with strain, which have been discussed previously. The significant resistance changes are mainly due to the increase in the inter-particle distance and decrease in the GnPs sheets interconnection. As the strain increases these factors overlap. Furthermore, the resistance decreases when the content of GnPs in composite film is increased from low content (1.25%) to high content (5%). This is because 5 vol % GnPs composite film have higher electrical conductivity when compared to its peer low GnPs content composite film under the same strain. By contrast, the black curve (1.25%) shows the highest resistance change among all other curves under the same strain. A similar trend is observed for the gauge factor changes in Figure 9(d). In summary, the film with 1.25% content of GnPs shows higher gauge factor than others, although with the highest resistance change. Therefore, based on both mechanical performance tests and gauge factor measurement, high-content GnPs film has lower sensitivity but stable productivity and better mechanical performance. We chose the composite film with 2.5% content GnPs composite film as the subject of the following study due to the ideal mechanical performance and sensitivity.

We then conducted cyclic tensile test to study the stability and reproducibility of sensor. The sensor exhibits good durability after 1000 cycles at 10% in Figure 10. The resistance changes of first 20 second and last 20 second were compared, suggesting the sensor has good stability and reproducibility. In addition, it almost instantaneously responds to cyclic loading, indicating it has quick response ability. All of the performances stated above are beneficial to our flexible strain sensor.

We firstly applied the sensors under a normal condition of pulse movement with the speed of 1.5 beats/s [Figure 11(a)]. Our strain

sensor can clearly and instantaneously monitor pulse movement, which is essential to diagnose in some medical conditions. Each recorded pulse cycle includes (1) a wave corresponding to the

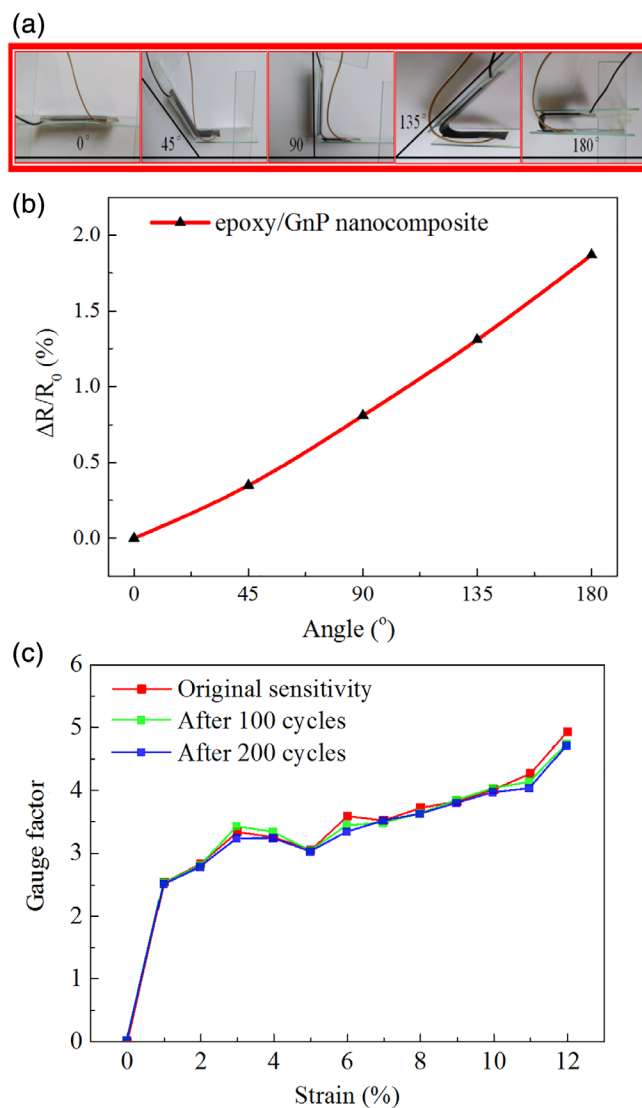


Figure 12. A flexible sensor with various (a) bending angles; (b) resistance change rates, and (c) the gauge factor after several bending. [Color figure can be viewed at wileyonlinelibrary.com]

incident forward wave, (2) a relative steady section originating from the diastolic wave,^{36,38} and (3) a minor dicrotic notch.³⁹ Second, our sensor can clearly detect the stretched forearm skin caused by fist clenching, forming a signal of resistance enhancement ~50% which relates to a peak in Figure 11(b); the peak should correspond to the initial clenching, and the progressive decline of resistance is explained by elastic recovery of the skin.

Flexible Sensors

Previous experiments in the sensing section mainly focused on the change of resistance rate during stretching, and our films also have certain sensing properties when bending. In this part, 2.5% content composite film has been used. The performance of the epoxy/GnP composite films with 2.5% of GnPs under different bending conditions is illustrated in Figure 12(a). As shown in Figure 12(a), composite films could be bent up to 180°, demonstrating good flexibility. The resistance changes rate graphs in Figure 12(b) demonstrate variation with bending angles of 45°, 90°, 135°, and 180°. It can be seen from the Figure 12(b) that the response of a larger angle is more sensitive than for a small bending angle. This may be due to the fact that the GnPs sheets at the bend become denser as the bending angle increases, which makes the sensing ability more sensitive. We then conducted cyclic tensile test to study the stability and reproducibility of sensor. In Figure 12, the resistance changes of 100 bending cycles and 200 bending cycles were compared, suggesting the sensor has good stability and repeatability.

CONCLUSION

In summary, we used a novel method to make the epoxy/GnP composite film by adding the flexible curing agent J2000. J2000 has long molecular chains that can attach more functional particles to improve the uptake of functional particles. The cured composite has good flexibility and ductility. With the increased content of GnPs, the conductivity of composite film improves from 10^{-14} to 10^{-6} S/cm. Epoxy/GnP composites also show generally prominent increase in Young's modulus and tensile strength at higher GnPs level. As a flexible sensor, it successfully achieved real-time monitoring for several body motions such as pulse movement and muscle deformation clearly demonstrating the potential of the composite film as a flexible sensor.

ACKNOWLEDGMENT

The authors thank Asbury and Huntsman (China) for providing the graphite intercalation compounds and Jeff amine D 400, respectively. This work was financially supported by the Natural Science Foundation of Liaoning Province (20170520142). Dr. Tianqing Liu is supported by NHMRC Early Career Fellowship (1112258). The authors are grateful to Dr. Jason Connor from School of Chemical Engineering, the University of Adelaide for useful suggestions to the manuscript.

REFERENCES

- Tang, L.; Ying, W.; Li, Y.; Feng, H.; Jin, L.; Li, J. *Adv. Funct. Mater.* **2010**, *19*(17), 2782.
- Meng, Q.; Hao, W.; Zhao, Z.; Araby, S.; Lu, S.; Ma, J. *Compos. Part A Appl. Sci. Manuf.* **2017**, *92*, 42.
- Lu, L.; Hou, W.; Sun, J.; Wang, J.; Qin, C.; Dai, L. *J. Mater. Sci.* **2014**, *49*(9), 3322.
- Ghaleb, Z. A.; Mariatti, M.; Ariff, Z. M. *Compos. Part A Appl. Sci. Manuf.* **2014**, *58*(3), 77.
- Kim, K. W.; Kim, D. K.; Kim, B. S.; An, K. H.; Park, S. J.; Rhee, K. Y.; Kim, B. J. *Compos. Part B Eng.* **2017**, *112*, 15.
- Chand, S. *J. Mater. Sci.* **2000**, *35*(6), 1303.
- Mohan, P. *J. Macromol. Sci.: Part D Rev. Polym. Process.* **2013**, *52*(2), 107.
- Chun, K. Y.; Oh, Y.; Rho, J.; Ahn, J. H.; Kim, Y. J.; Choi, H. R.; Baik, S. *Nat. Nanotechnol.* **2010**, *5*(12), 853.
- Li, J.; Man, L. S.; Kim, J. K.; Marom, G. *Compos. Sci. Technol.* **2007**, *67*(2), 296.
- Balageas, D.; Fritzen, C. P.; Güemes, A. *Struct. Eng. Mech. Comput.* **2001**, *6531*(8), 1185.
- Chiauszi, E.; Rodarte, C.; Dasmahapatra, P. *BMC Med.* **2015**, *13*(1), 77.
- Pötzelberger, I.; Mardare, A. I.; Hassel, A. W. *Appl. Surf. Sci.* **2017**, *417*, 48.
- Ahmed, M.; Chitteboyina, M. M.; Butler, D. P.; Çelik-Butler, Z. *IEEE Sensors J.* **2013**, *13*(10), 4081.
- Wang, Y.; Wu, J.; Wei, F. *Carbon.* **2003**, *41*(15), 2939.
- Siddiqui, N. A.; Sham, M. L.; Tang, B. Z.; Munir, A.; Kim, J. K. *Compos. Part A Appl. Sci. Manuf.* **2009**, *40*(10), 1606.
- Stoller, M. D.; Park, S.; Zhu, Y.; An, J.; Ruoff, R. S. *Nano Lett.* **2008**, *8*(10), 3498.
- Lee, C.; Wei, X.; Kysar, J. W.; Hone, J. *Science.* **2008**, *321* (5887), 385.
- A.A. Balandin, S. Ghosh, W. Bao, I. Calizo, D. Teweldebrhan, F. Miao, C.N. Lau, Extremely High Thermal Conductivity of Graphene: Experimental Study, Eprint Arxiv (2008).
- Scarpa, F.; Adhikari, S.; Srikantha, P. A. *Nanotechnology.* **2009**, *20*(6), 065709.
- T.p.m.c.n.c.T. properties, nanoindentation. *J. Appl. Polym. Sci.* **2015**, *131*(23), 205.
- KUILA, T.; KHANRA, P.; Mishra, K.; Anata, N. H. K.; Lee, J. H. *Polym. Testing.* **2012**, *31*(2), 282.
- Silva, W. M. D.; Ribeiro, H.; Neves, J. C.; Calado, H. D. R.; Garcia, F. G.; Silva, G. G. *J. Therm. Anal. Calorimetry.* **2014**, *115*(2), 1021.
- Liu, Y. J.; Chen, X. L. *Mech. Mater.* **2003**, *35*(1), 69.
- Schueler, R.; Petermann, J.; Schulte, K.; Wentzel, H. P. *Macromol. Symp.* **1996**, *104*(104), 261.
- Shuan, H.; Zhao, J.; Chen, H. *J. Mater. Sci. Technol.* **2016**, *32*(5), 425.
- Chatterjee, S.; Wang, J. W.; Kuo, W. S.; Tai, N. H.; Salzmann, C.; Li, W. L.; Hollertz, R.; Nüesch, F. A.; Chu, B. T. T. *Chem. Phys. Lett.* **2012**, *531*(13), 6.
- Ma, J.; Meng, Q.; Zaman, I.; Zhu, S.; Michelmores, A.; Kawashima, N.; Wang, C. H.; Kuan, H. C. *Compos. Sci. Technol.* **2014**, *91*(2), 82.
- Tang, G.; Jiang, Z. G.; Li, X.; Zhang, H. B.; Yu, Z. Z. *Chin. J. Polym. Sci.* **2014**, *32*(8), 975.

29. Zaman, I.; Kuan, H. C.; Dai, J.; Kawashima, N.; Michelmore, A.; Sovi, A.; Dong, S.; Luong, L.; Ma, J. *Nanoscale*. **2012**, *4*(15), 4578.
30. Abot, J. L.; Yi, S.; Vatsavaya, M. S.; Medikonda, S.; Kier, Z.; Jayasinghe, C.; Rooy, N.; Shanov, V. N.; Schulz, M. J. *Compos. Sci. Technol.* **2010**, *70*(7), 1113.
31. Cristina, V.; Carlos, D.; Hassan, S.; Furtado, C. A.; Maoshuai, H.; Olivier, R.; Luca, O.; Marc, M.; Alain, P. *J. Am. Chem. Soc.* **2008**, *130*(47), 15802.
32. Yenny, H.; Valeria, N.; Mustafa, L.; Blighe, F. M.; Zhenyu, S.; Sukanta, D.; McGovern, I. T.; Brendan, H.; Michele, B.; Gun'Ko, Y. K. *Nat. Nanotechnol.* **2008**, *3*(9), 563.
33. Ma, P. C.; Siddiqui, N. A.; Marom, G.; Kim, J. K. *Compos. Part A Appl. Sci. Manuf.* **2010**, *41*(10), 1345.
34. Qingshi, M.; Jian, J.; Ruoyu, W.; Hsu-Chiang, K.; Jun, M.; Nobuyuki, K.; Andrew, M.; Shenmin, Z.; Wang, C. H. *Nanotechnology*. **2014**, *25*(12), 125707.
35. Li, J.; Ma, P. C.; Chow, W. S.; Chi, K. T.; Kim, J. K. *Adv. Funct. Mater.* **2010**, *17*(16), 3207.
36. Chunsheng, L.; Yiu-Wing, M. *Phys. Rev. Lett.* **2005**, *95*(8), 088303.
37. Celzard, A.; Mcrae, E.; Deleuze, C.; Dufort, M. *Phys. Rev. B Condens. Matter*. **1996**, *53*(10), 6209.
38. Meng, Q.; Wu, H.; Zhao, Z.; Araby, S.; Lu, S.; Ma, J. *Compos. Part A: Appl. Sci. Manuf.* **2017**, *92*, 42.
39. Yunker, P. J.; Tim, S.; Lohr, M. A.; Yodh, A. G. *Nature*. **2011**, *476*(7360), 308.
40. Sanghavi, B. J.; Wolfbeis, O. S.; Hirsch, T.; Swami, N. S. *Microchim. Acta*. **2015**, *182*(1-2), 1.
41. Zaman, I.; Manshoor, B.; Khalid, A.; Meng, Q.; Araby, S. *J. Mater. Sci.* **2014**, *49*(17), 5856.
42. Chhetri, S.; Adak, N. C.; Samanta, P.; Murmu, N. C.; Kuila, T. *Polym. Testing*. **2017**, *63*, 1.
43. Araby, S.; Meng, Q.; Zhang, L.; Kang, H.; Majewski, P.; Tang, Y.; Ma, J. *Polymer*. **2014**, *55*(1), 201.
44. Yang, H.; Yao, X.; Zheng, Z.; Gong, L.; Yuan, L.; Yuan, Y.; Liu, Y. *Compos. Sci. Technol.* **2018**, *167*, 371.